Pulsating laminar fully developed channel and pipe flows

Kais Haddad, Özgür Ertunç, Manoranjan Mishra, and Antonio Delgado
LSTM-Erlangen, Institute of Fluid Mechanics, Friedrich-Alexander-Universität Erlangen-Nürnberg, Cauerstrasse 4, D-91058 Erlangen, Germany

(Received 5 January 2009; published 8 January 2010)

Analytical investigations are carried out on pulsating laminar incompressible fully developed channel and pipe flows. An analytical solution of the velocity profile for arbitrary time-periodic pulsations is derived by approximating the pulsating flow variables by a Fourier series. The explicit interdependence between pulsations of velocity, mass-flow rate, pressure gradient, and wall shear stress are shown by using the proper dimensionless parameters that govern the flow. Utilizing the analytical results, the scaling laws for dimensionless pulsation amplitudes of the velocity, mass-flow rate, pressure gradient, and wall shear stress are analyzed as functions of the dimensionless pulsation frequency. Special attention has been given to the scaling laws describing the flow reversal phenomenon occurring in pulsating flows, such as the condition for flow reversal, the dependency of the reversal duration, and the amplitude. It is shown that two reversal locations away from the wall can occur in pulsating flows in pipes and channels and the reversed amount of mass per period reaches a maximum at a certain dimensionless frequency for a given amplitude of mass-flow rate fluctuations. These analyses are numerically conducted for pipe and channel flows over a large frequency range in a comparative manner.

DOI: 10.1103/PhysRevE.81.016303 PACS number(s): 47.10.−g, 47.15.Rq

I. INTRODUCTION

In nature and technological applications, transport of mass and energy via fluid flow are unsteady. However, time-dependent effects have been discarded in the fluid mechanics investigations when researchers confronted the nonlinear complexity of the fluid flow. As a result of high complexity, unavailability of fast response measurement techniques and resources for numerical simulations, time effect on the flow-related phenomena remained a niche for research and, even more, for development. Comprehensive understanding of the dynamics of the time-dependent flows would allow the exploitation of a large spectrum of processes by provoking unsteady mass, momentum, and energy transfer with guided unsteady dynamics.

Time-dependent and, especially, time-periodic flows seem to be more advantageous for achieving higher values of flow properties when compared to steady flow processes in many circumstances. For example, the appearance of periodic peaks of wall shear stress in a time-periodic internal flow may enhance mass transport through permeable walls or enhance both the removal and prevention of deposits within the piping used in the processing of biomaterial [1]. Catalysts, which have an extremely high number of conduits, were shown to provide more favorable conditions for the catalytic process performance under unsteady operation [2,3]. The benefits of unsteady flows on heat transfer for different applications are controversially discussed in the literature [4–6]. Enhancement as well as reduction in heat transfer in pulsating pipe and channel flows were reported depending on the parameter set studied. It has been known that oscillatory flows influence the dispersion of particles or contaminants in oscillating flows [7,8]. In contrast to these mixing examples, Thomas and Narayanan [9] showed that pulsating flows can be utilized to separate species in a flow. Intake and exhaust manifolds of internal combustion engines, respiratory and circulatory systems are some of the real life examples of pulsating internal flows, which incorporate branching conduits. Recent studies on physiological systems accented the important role of time-dependent flows. The understanding of time-dependent flow along the bronchial tree down to alveoli [10,11] is of vital importance for the development of mechanical ventilation devices and the selection of optimizing the breathing maneuvers for each patient [12,13]. The connection between the arterial flow pressure and arterial flow rate [14,15], the effect of unsteady hydrodynamic loads on the occurrence, development and treatment of aneurysms [16], and response of body to pulsatile and nonpulsatile artificial heart or ventricular assist device [17], are examples of pending questions relevant to the time-periodic nature of circulatory system. Modeling of oscillatory flow of cerebrospinal fluid (CSF) in the brain [18] and in the branches of the uterine artery [19] are recent examples of time-dependent flow investigations relevant to physiology.

In spite of its high technical and medical relevance, some of the observed effects of time-periodic flows are not sufficiently supported by the theory. Investigations of pulsating flows in conduits with simple geometries, like pipe and channel, provided fundamental information on understanding the time-dependent internal flows. In spite of the fact that analytical and experimental studies on pulsating incompressible laminar flows through pipes and channels started in 1930 (for a review, see Gündogdu and Çarpınlıoglu [20] and Ünsal *et al.* [21]), only recently, have comprehensive analytical solutions for transient flows [22–24] and arbitrary time-periodic flows [25–27] been obtained. The solution method in these studies were based on either a Laplace transform [22,24,26] or on a Fourier series [25,27]. It is important to note that in contrast to the solutions based on the Laplace transform, the Fourier series approach, which roots back to Uchida [28], can handle only time-periodic flows. Among those studies, only Brereton [24] for transient flows and Ray *et al.* [27] for arbitrary time-periodic flows showed the interdependence of

flow quantities. For example, Ray *et al.* [27] provided the relationship between arbitrary time-periodic mass-flow rate pulsations and the pulsations of the pressure gradient in a pipe as well as for the ducts of arbitrary cross sections [29,30]. In the aforementioned studies, the scaling laws between various flow quantities were rarely analyzed to an extend that these laws can directly be used in a practical flow process. In contrary to those, a good example is the development of flow rate metering device for motor injection systems [31] based on the relationship between the mass-flow rate and pressure pulsations obtained by Ray *et al.* [27].

An important phenomena in pulsating flows is flow reversal, i.e., the coexistence of positive and negative flow velocities in a profile at an instant in time. Looking at these various applications, it is very much essential to understand and quantify details about the flow reversal phenomena through the analytical results. To the authors' knowledge, there is an unavailability of any extensive quantitative study in the literature. It has been shown (see, for example, [21]) that this flow reversal begins near the wall for high pulsation frequency. In order to obtain more insights into flow reversal, we have studied in detail both the channel as well as the pipe case and a comparison of the results are presented here, which can be useful in understanding the flow reversal.

Having in mind the various applications of time-dependent flow processes such as flow rate metering, deposition removal, etc., the main objective of this article is a consolidation of the understanding on laminar incompressible fully developed pulsating channel and pipe flows and related scaling law. For this purpose, first, based on the Fourier series, we provide a general analytical solution for the velocity, which is valid for laminar arbitrarily pulsating pipe and channel flows. Considering only incompressible flows, equations for the pulsating velocity, mass-flow rate, pressure gradient, and wall shear stress are derived involving the explicit dependence between all those quantities. The analytical solution follows the methodology provided by Ray *et al.* [27] for pipe flows. Later, special attention is given to flows with sinusoidal pulsations of mass-flow rate. Accordingly, we simplify the general solution and summarize the basic equations for pipe and channel flows with sinusoidal pulsations. Finally, we analyze numerically in detail the scaling laws for the ratio between the flow rate amplitude and the pressure gradient amplitude, the wall shear stress and, especially the peculiarities of the flow reversal. Comparison between the pipe and the channel flows are provided throughout the analysis.

II. ANALYTICAL SOLUTIONS OF PULSATING CHANNEL AND PIPE FLOWS

The analytical solutions of laminar pulsating flows in a pipe and channel driven by an unsteady pressure gradient are studied by Uchida [28] and Majdalani and Chibli [25], respectively. Even though the analytical solution for the pipe flows for a prescribed mass-flow rate pulsation instead of pressure gradient are given by Ray *et al.* [27], it is essential to understand such a flow in both pipe and channel geometry using a conventional form of the equation and deriving the properties of the solutions in dimensionless form in order to compare in both cases of pipe and channel flows. We write the governing equations (the continuity equation and the Navier-Stokes equation) for unsteady fully developed laminar parallel flows of an incompressible Newtonian fluid as [24]

$$\frac{\partial u}{\partial x} = 0, \tag{1}$$

$$\frac{\partial u}{\partial t} = -\frac{1}{\rho}\frac{\partial p}{\partial x} + \frac{\nu}{r^k}\frac{\partial}{\partial r}\left(r^k \frac{\partial u}{\partial r}\right), \tag{2}$$

$$\frac{1}{\rho}\frac{\partial p}{\partial r} = 0, \tag{3}$$

where u, p, ρ, and ν are the axial velocity, pressure, density, and kinematic viscosity, respectively. The parameter $k=0$, and 1 corresponds to the Cartesian (channel flows with walls at $r=\pm R$) and axisymmetric (pipe flow) coordinate system, respectively. From Eq. (3) and the fully developed flow condition, it can be found that the pressure gradient depends only on time t. So, we prescribe the driving pressure gradient in the form of a Fourier series as

$$-\frac{1}{\rho}\frac{\partial p}{\partial x} = p_0 + \Re\left\{\sum_{n=1}^{\infty} p_n \exp(2\pi n f t i)\right\}, \tag{4}$$

where p_0 is the steady part of the pressure gradient, $p_n = p_{cn} - i p_{sn}$ with p_{cn} and p_{sn} representing the cosine and sine amplitudes of the harmonic function, and f is the overall frequency of pulsation. $\Re$ is symbolizing the real part of the complex function.

To nondimensionalize the governing flow equation, we use $t_c = R^2/\nu$ (time scale of viscous diffusion of momentum) as a characteristic time scale and the characteristic pressure gradient can be defined with the average velocity [27], $\left(-\frac{1}{\rho}\frac{\partial p}{\partial x}\right)_c = \frac{\nu u_{\mathrm{av}}}{R^2}$. The dimensionless quantities are then defined as

$$u^* = \frac{u}{u_{av}}, \quad r^* = \frac{r}{R}, \quad p_n^* = \frac{p_n}{p_0}, \quad \left(-\frac{1}{\rho}\frac{\partial p}{\partial x}\right)^* = \frac{\left(-\frac{1}{\rho}\frac{\partial p}{\partial x}\right)}{\left(-\frac{1}{\rho}\frac{\partial p}{\partial x}\right)_c},$$

$$\tau = \frac{t}{t_c}, \quad F = f t_c, \tag{5}$$

where u_{av} is the average velocity of the fluid through the pipe ($u_{\mathrm{av}} = p_0 R^2/8\nu$) or channel ($u_{\mathrm{av}} = p_0 R^2/3\nu$) corresponding to the steady part of the pressure gradient. By dropping the exponent (*) from the dimensionless variables the nondimensional equation of motion (2) becomes

$$\frac{\partial u}{\partial \tau} = -\frac{1}{\rho}\frac{\partial p}{\partial x} + \frac{1}{r^k}\frac{\partial}{\partial r}\left(r^k \frac{\partial u}{\partial r}\right), \tag{6}$$

with

$$-\frac{1}{\rho}\frac{\partial p}{\partial x} = \begin{cases} 3\left(1+\Re\left\{\sum_{n=1}^{\infty} p_n \exp(2\pi nF\tau i)\right\}\right), & \text{for channel} \\ 8\left(1+\Re\left\{\sum_{n=1}^{\infty} p_n \exp(2\pi nF\tau i)\right\}\right), & \text{for pipe} \end{cases}. \tag{7}$$

The governing equations need to be solved for the channel ($k=0$) and the pipe ($k=1$) case separately. The velocity u can be sought similarly to the Fourier series expansion of pressure gradient, as $u=u_0(r)+\Re\{\Sigma_{n=1}^{\infty}u_n(r)\exp(2\pi nF\tau i)\}$. Introducing the above expansion of u into the Eq. (6), for channel case $k=0$, and by collecting the steady and unsteady part separately with the no-slip boundary conditions at the wall $r=\pm 1$, the fluid flow solution can be obtained. In the present paper we would like to analyze the results in comparison to the solution of pulsating pipe flows which is known in terms of Bessel Functions, hence, we write the solution in terms of Bessel functions instead of the traditional hyperbolic functions [25], using the known relations $[\cosh(r)=\sqrt{i\pi r/2}J_{-1/2}(ir), \sinh(r)=-i\sqrt{i\pi r/2}J_{1/2}(ir)]$, as

$$u=\frac{3}{2}(1-r^2)+\Re\left\{\frac{3}{2}\sum_{n=1}^{\infty}\frac{ip_n}{\pi nF}\left[\frac{\sqrt{r}J_{-1/2}(i^{3/2}r\sqrt{2\pi nF})}{J_{-1/2}(i^{3/2}\sqrt{2\pi nF})}-1\right]\times\exp(2\pi nF\tau i)\right\}. \tag{8}$$

Similarly following [27], the mass-flow rate $\dot{m}$ normalized by the mean flow rate $\dot{m}_M=2\rho bRu_{\text{av}}$, where b is the depth of the channel, become

$$\dot{m}=1-\Re\left\{\frac{3}{2}\sum_{n=1}^{\infty}\frac{ip_n}{\pi nF}\left[\frac{\sqrt{i}J_{1/2}(i^{3/2}\sqrt{2\pi nF})}{\sqrt{2\pi nF}J_{-1/2}(i^{3/2}\sqrt{2\pi nF})}+1\right]\times\exp(2\pi nF\tau i)\right\}. \tag{9}$$

From the equation above one can find p_n if $\dot{m}$ is known. Equation (9) can be analyzed further, considering without loss of generality only the sine term from the Eq. (4) [27], i.e., $p_n=-ip_{sn}$, by writing in a convenient form $\dot{m}=1+\Sigma_{n=1}^{\infty}\dot{m}_{os,n}$, where

$$\dot{m}_{os,n}=\Re\left\{-\frac{3}{2}\frac{p_{sn}}{\pi nF}\left[\frac{\sqrt{i}J_{1/2}(i^{3/2}\sqrt{2\pi nF})}{\sqrt{2\pi nF}J_{-1/2}(i^{3/2}\sqrt{2\pi nF})}+1\right]\times\exp(2\pi nF\tau i)\right\}, \tag{10}$$

is the n^{th} oscillating part of the pulsating mass-flow rate. By extracting a complex variable $\psi_{m,n}(nF)$ from Eq. (10) [27],

$$\psi_{m,n}(nF)=-\frac{3}{2\pi nF}\left[\frac{\sqrt{i}J_{1/2}(i^{3/2}\sqrt{2\pi nF})}{\sqrt{2\pi nF}J_{-1/2}(i^{3/2}\sqrt{2\pi nF})}+1\right], \tag{11}$$

and after some algebra using the relations $a\cos\theta-b\sin\theta=\sqrt{a^2+b^2}\sin[\theta-\tan^{-1}(a/b)]$, the mass-flow rate $\dot{m}$ becomes

$$\dot{m}=1+\sum_{n=1}^{\infty}p_{sn}|\psi_{m,n}|\sin\left[2\pi nF\tau-\tan^{-1}\left\{\frac{\Re(\psi_{m,n})}{\Im(\psi_{m,n})}\right\}\right], \tag{12}$$

where $\Re(\psi_{m,n})$ and $\Im(\psi_{m,n})$ are the real and imaginary parts of the complex variable. Equation (12) can be rewritten as

$$\dot{m}=1+\sum_{n=1}^{\infty}\dot{m}_n\sin(2\pi Fn\tau+\Delta\theta_{m,n}), \tag{13}$$

where

$$\dot{m}_n=p_{sn}|\psi_{m,n}|, \tag{14}$$

$$\Delta\theta_{m,n}=-\tan^{-1}\left\{\frac{\Re(\psi_{m,n})}{\Im(\psi_{m,n})}\right\} \tag{15}$$

are the amplitude and phase lag (between the pressure pulsation and the mass-flow rate) of the n^{th} wave of the mass-flow rate oscillation and an interesting observation is that both the amplitude ratio and phase lag are functions of the n^{th} frequency, nF. Equations (14) and (15) give the interdependence of the pressure gradient and mass-flow rate pulsations. In other words, knowing the pressure gradient pulsations, one can obtain the pulsation of mass-flow rate or vice versa. As explained by Ray *et al.* [27], if the prescribed mass-flow rate pulsations are of the form $\dot{m}=1+\Sigma_{n=1}^{\infty}\dot{m}_n\sin(2\pi nF\tau)$, then using Eqs. (14) and (15) and following Eq. (7), we can get the pressure gradient pulsation as

$$-\frac{1}{\rho}\frac{\partial p}{\partial x}=3\left\{1+\sum_{n=1}^{\infty}p_{sn}\sin(2\pi nF\tau-\Delta\theta_{m,n}),\right\},$$

which has additional phase lag $\Delta\theta_{m,n}$. Hence, for the prescribed mass-flow rate pulsation the velocity can be obtained as

$$u=\frac{3}{2}(1-r^2)+\Re\left\{\frac{3}{2}\sum_{n=1}^{\infty}\frac{p_{sn}}{\pi Fn}\left[\frac{\sqrt{r}J_{-1/2}(i^{3/2}r\sqrt{2\pi Fn})}{J_{-1/2}(i^{3/2}\sqrt{2\pi Fn})}-1\right]\times\exp[(2\pi nF\tau-\Delta\theta_{m,n})i]\right\}. \tag{16}$$

Following a similar analysis of all through the Eqs. (9)–(15), without loss of generality, one can write the velocity of pulsating flows Eq. (16) by normalizing with the steady part of the velocity $[\frac{3}{2}(1-r^2)]$ and superposition of sinusoidal wave forms as

$$U = \frac{u}{\frac{3}{2}(1-r^2)} = 1 + \sum_{n=1}^{\infty} u_{A,n} \sin(2\pi Fn\tau - \Delta\theta_{m,n} + \Delta\theta_{u,n}), \tag{17}$$

where

$$u_{A,n} = p_{sn}|\psi_{u,n}|, \tag{18}$$

$$\Delta\theta_{u,n} = \tan^{-1}\left\{\frac{\Re(\psi_{u,n})}{\Im(\psi_{u,n})}\right\}, \tag{19}$$

$$\psi_{u,n}(nF) = \frac{1}{\pi Fn(1-r^2)}\left[\frac{\sqrt{r}J_{-1/2}(i^{3/2}r\sqrt{2\pi Fn})}{J_{-1/2}(i^{3/2}\sqrt{2\pi Fn})} - 1\right]. \tag{20}$$

The phase angle $\Delta\theta_{u,n}$ is the phase lag between pressure gradient and velocity at different transverse position r through the cross section of the channel and $u_{A,n}$ is the amplitude of the velocity. Similarly, the dimensionless wall shear stress τ_w can be obtained in terms of sinusoidal forms with a phase lag $\Delta\theta_{s,n}$ between pressure gradient and shear stress and the detail form of the τ_w for a sinusoidal pulsation is given in Table I.

Since in this paper, the aim of our study is to compare the results of pipe as well as channel for prescribed sinusoidal mass-flow rate pulsation $\dot{m}=1+\dot{m}_A \sin(2\pi F\tau)$, so a table (Table I) is prepared for the important quantities of interest, i.e., velocity, wall shear stress, and for the interdependence relations of mass-flow and pressure gradient. The above described solutions Eqs. (12)–(20) become valid for sinusoidal pulsations by taking $n=1$. The pipe flows ($k=1$) solutions can be obtained in the same procedure as described for channel case ($k=0$) and already available in literature [27]. It is worth noting that the measurements of the velocity at the center of channel for a wide range of $\dot{m}_A$ and F, by Haddad [32], were in good agreement with the analytical results.

III. COMPARISON OF PHYSICAL QUANTITIES IN BOTH CHANNEL AND PIPE FLOWS

As channels and pipes are common geometries utilized in many flow processes, it is important to know the effect of the conduit shape on the dynamics of the pulsating flows. Moreover, sinusoidal pulsations represent many features of time-periodic pulsations, which are used in many applications. Therefore, we perform analysis of the analytical solutions for both the pipe and the channel for sinusoidal pulsations. In this section, parameters of technical interest such as the pressure waveforms, maximum and minimum wall shear stress values, and, in the next section, flow reversal phenomenon are considered in terms of dimensionless parameters and comparisons for pipe and channel flows are provided.

A. Pressure waveforms

The applied mass-flow rate pulsations and the corresponding pressure gradients per unit mass, which were calculated by using the analytical solutions, are presented in Fig. 1. For the same mass-flow rate, the dimensionless frequency F, is varied over the range 0.01–10. Figure 1 shows that increasing F, causes the amplitude of the pressure gradient to increase for both pipe and channel flows. At low frequencies, the phase shift between the input and output signals does not exit, however, at higher frequencies a shift appear and increases with increasing F. It also appears from Fig. 1 that for a channel flow, the resulted pressure waveforms have higher amplitude than that for the pipe flow.

Figure 2(a) shows the variation in $\dot{m}_A/P_A$ and $\Delta\theta_m$ with F for both pipe and channel flows. This figure indicates also that there are three different flow regimes. The first regime is referred to as the low frequency regime at which the time scale of the induced pulsations $(1/f)$ are longer than the viscous time scale (t_c) so that flow can follow the given pulsations without any retardation in time. Therefore, it is characterized by a constant amplitude ratio, which is equal to unity, and negligible phase shift. In the second regime, the time scale of pulsations reduces down to that of the viscous time scale, so that the momentum distribution across the conduit cannot follow the changes in the mass-flow rate without retarding. In other words, viscous diffusion of momentum throttles the flow and, consequently, higher amplitudes of pressure pulsations are necessary with increasing F for a given mass-flow rate pulsation. Hence, the amplitude ratio is decreasing while the phase shift increases, both in a rapid manner. At very high frequencies the rate of change in the amplitude ratio is very small and $\dot{m}_A/P_A$ tends to zero while the phase shift asymptotically tends to $\pi/2$.

It can be concluded from Fig. 2(a) that in the intermediate regime and at the same F, the amplitude ratio, $\dot{m}_A/P_A$, for channel flow is lower, which means that $P_{A_{\mathrm{Ch}}}$ is always higher than $P_{A_{\mathrm{Pipe}}}$ for the same mass-flow rate pulsation. Regarding the phase shift, it is obvious that in the same regime, the value of $\Delta\theta_m$ for the channel flow is larger than that for the pipe. The change in $P_{A_{\mathrm{Ch}}}/P_{A_{\mathrm{Pipe}}}$ as a function of F is depicted in Fig. 2(b). The ratio is almost 1 up to $F\sim 0.1$, and then it increases very fast up to $F\sim 2.5$ and the rate of increase slows down at higher frequencies F.

B. Velocity evolution and its characteristics

Instantaneous velocity profiles give deeper insight about the effect of the pulsation frequency. The theoretically calculated velocity profiles for $F=0.1$, 1, 3, 30, and $\dot{m}_A=0.7$ for channel flow are presented in Fig. 3. With increasing F for $F=0.1$, 1.0, and 3, flattening of the velocity profile can be observed at the center. At $F=3$, there is a weak flow reversal in the vicinity of the wall and it becomes more visible at $F=30$. As the flow reversal occurs first on the wall, the velocity profile has one inflection point in one half of the conduit. All the previous studies pointed out that reversal can happen only near the wall. However, the present study shows that for higher F, reversal can occur in a region shifted slightly from the wall. In other words, one can observe two inflection points in the velocity profile of the half conduit height. Figure 4 reveals this fact. It can be seen that for the phase $10.5\pi/6$, the velocity profile is characterized by two inflec-

TABLE I. A comparison between the nondimensional quantities of interest, mass-flow rate m, Velocity U, sinusoidal pressure pulsation amplitude P_A, wall shear stress τ_w for both pipe, and channel flows with a prescribed sinusoidal mass-flow rate pulsation.

Quantity of interest	Pipe	Channel
$\dot{m}$	$\dot{m}=1+\dot{m}_A \sin(2\pi F\tau)$	$\dot{m}=1+\dot{m}_A \sin(2\pi F\tau)$
Pressure gradient ∇P	$\nabla P=-\frac{1}{8\rho}\frac{\partial p}{\partial x}=1+P_A \sin(2\pi F\tau-\Delta\theta_m)$	$\nabla P=-\frac{1}{3\rho}\frac{\partial p}{\partial x}=1+P_A \sin(2\pi F\tau-\Delta\theta_m)$
	$P_A=\frac{\dot{m}_A}{\lvert\psi_m\rvert}$	$P_A=\frac{\dot{m}_A}{\lvert\psi_m\rvert}$
	$\psi_m(F)=-\frac{4}{\pi F}\left[\frac{2\sqrt{i}J_1(i^{3/2}\sqrt{2\pi F})}{\sqrt{2\pi F}J_0(i^{3/2}\sqrt{2\pi F})}+1\right]$	$\psi_m(F)=-\frac{3}{2\pi F}\left[\frac{\sqrt{i}J_{\frac{1}{2}}(i^{3/2}\sqrt{2\pi F})}{\sqrt{2\pi F}J_{-\frac{1}{2}}(i^{3/2}\sqrt{2\pi F})}+1\right]$
	$\Delta\theta_m=-\tan^{-1}\left\{\frac{\Re(\psi_m)}{\Im(\psi_m)}\right\}$	$\Delta\theta_m=-\tan^{-1}\left\{\frac{\Re(\psi_m)}{\Im(\psi_m)}\right\}$
Velocity	$u=2(1-r^2)\{1+u_A \sin(2\pi F\tau-\Delta\theta_m+\Delta\theta_u)\}$	$u=\frac{3}{2}(1-r^2)\{1+u_A \sin(2\pi F\tau-\Delta\theta_m+\Delta\theta_u)\}$
	$U=\frac{u}{2(1-r^2)}$	$U=\frac{u}{\frac{3}{2}(1-r^2)}$
	$u_A=P_A\lvert\psi_u\rvert$	$u_A=P_A\lvert\psi_u\rvert$
	$\Delta\theta_u=\tan^{-1}\left\{\frac{\Re(\psi_u)}{\Im(\psi_u)}\right\}$	$\Delta\theta_u=\tan^{-1}\left\{\frac{\Re(\psi_u)}{\Im(\psi_u)}\right\}$
	$\psi_u(F)=\frac{2}{\pi F(1-r^2)}\left[\frac{J_0(i^{3/2}r\sqrt{2\pi F})}{J_0(i^{3/2}\sqrt{2\pi F})}-1\right]$	$\psi_u(F)=\frac{1}{\pi F(1-r^2)}\left[\frac{\sqrt{r}J_{-\frac{1}{2}}(i^{3/2}r\sqrt{2\pi F})}{J_{-\frac{1}{2}}(i^{3/2}\sqrt{2\pi Fn})}-1\right]$
Wall shear stress	$\tau_w=1+\tau_{w,A}\sin(2\pi F\tau+\Delta\theta_\tau)$	$\tau_w=1+\tau_{w,A}\sin(2\pi F\tau+\Delta\theta_\tau)$
	$\tau_{w,A}=P_A\lvert\psi_s\rvert$	$\tau_{w,A}=P_A\lvert\psi_s\rvert$
	$\Delta\theta_\tau=\Delta\theta_s-\Delta\theta_m$	$\Delta\theta_\tau=\Delta\theta_s-\Delta\theta_m$
	$\Delta\theta_s=\tan^{-1}\left\{\frac{\Re(\psi_s)}{\Im(\psi_s)}\right\}$	$\Delta\theta_s=\tan^{-1}\left\{\frac{\Re(\psi_s)}{\Im(\psi_s)}\right\}$
	$\psi_s(F)=-\frac{2i^{3/2}}{\sqrt{2\pi F}}\left[\frac{J_{-1}(i^{3/2}\sqrt{2\pi F})}{J_0(i^{3/2}\sqrt{2\pi F})}\right]$	$\psi_s(F)=-\frac{1}{\sqrt{2\pi Fi}}\left[\frac{J_{\frac{1}{2}}(i^{3/2}\sqrt{2\pi F})}{J_{-\frac{1}{2}}(i^{3/2}\sqrt{2\pi F})}\right]$

tion points, while at $7\pi/6$, one inflection point is observed. We call this reversal as *off-wall-reversal*. Flow reversal is treated in detail in Sec. IV.

Another set of investigations were carried out to study the change in u_A with F for different transverse locations across the channel. It is shown in Fig. 5(a) that u_A do not change with F in the same manner throughout the cross section. As u_A is the dimensionless velocity fluctuation amplitude normalized with the local steady component of the velocity fluctuation [see Eqs. (16) and (17)], u_A begins at the same value for a given mass-flow rate amplitude at all radial positions. There exists an interval of frequencies where the velocity amplitude deviates before it saturates to a constant value at higher frequencies F. This interval increases with increasing radial position from the center to near the wall. As the inertia of the flow is at most in the central region of the channel, velocity amplitude u_A strictly decreases at this interval with increasing F. In contrast to the central region of the channel, toward the wall, the inertia of the flow is less and therefore the flow can respond to the pulsation easily and, therefore, u_A rapidly increases with increasing F and has a maximum value before the saturation occurs. The change in u_A across

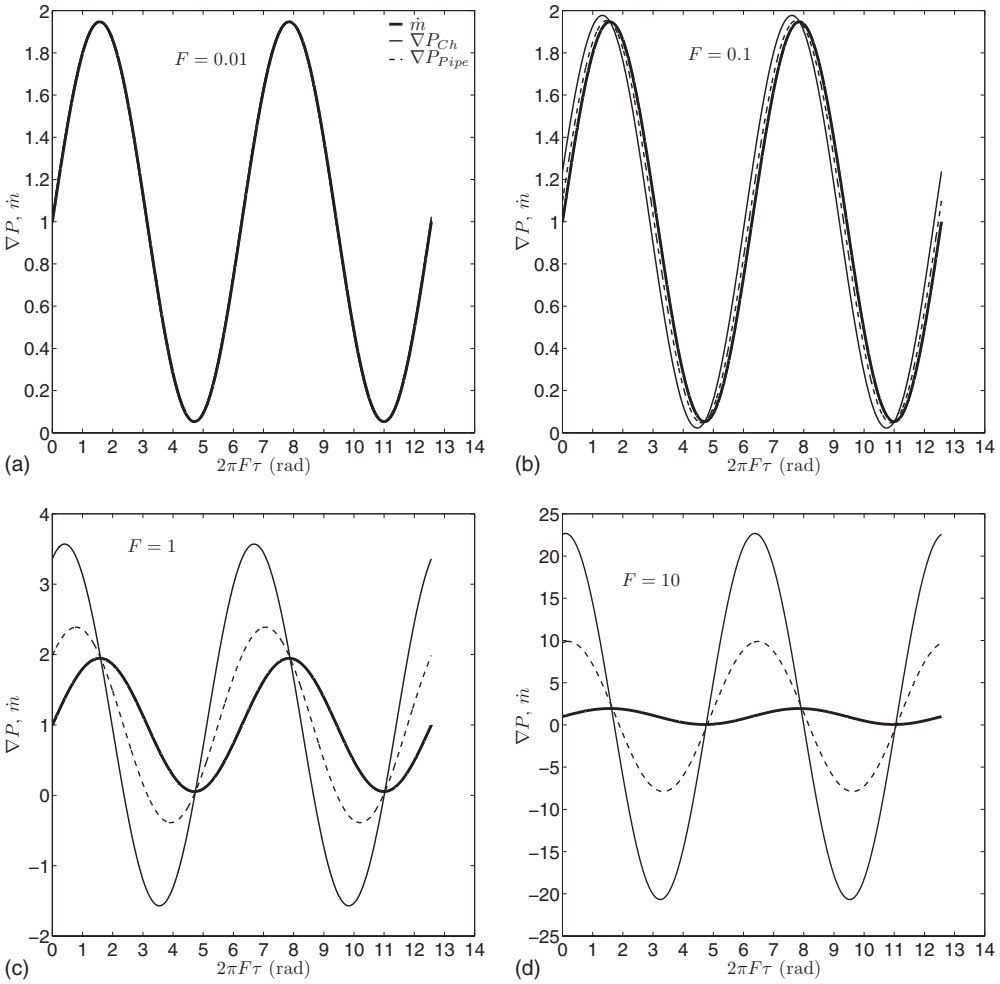

FIG. 1. The driving mass-flow rate ($\dot{m}$) and the pressure gradients (∇p) for different dimensionless pulsation frequencies (F) for channel and pipe flow.

the cross section with increasing F reveals that pulsations cause a redistribution of the momentum in the transverse direction.

Figure 5(b) shows the variation in the dimensionless velocity amplitude u_A with F for channel and pipe flows. For $F<2$, and at the centerline of the conduits, u_A is equal for both channel and pipe flows, whereas, for higher frequencies, the dimensionless amplitude for channel flow is higher than that for the pipe flow. On the other hand, near the wall u_A is always higher in the channel flow than in the pipe flow.

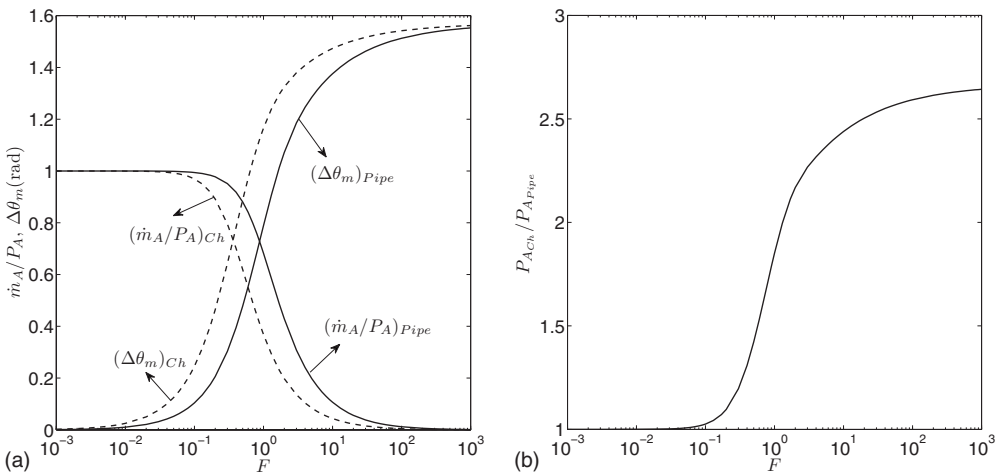

FIG. 2. (a) The variation in amplitude ratio, $\dot{m}_A/P_A$, and phase shift, $\Delta\theta_m$, with F for both channel (dashed line) and pipe (solid line). (b) The variation in dimensionless amplitude ratio, $P_{A_{\mathrm{Ch}}}/P_{A_{\mathrm{Pipe}}}$ with F.

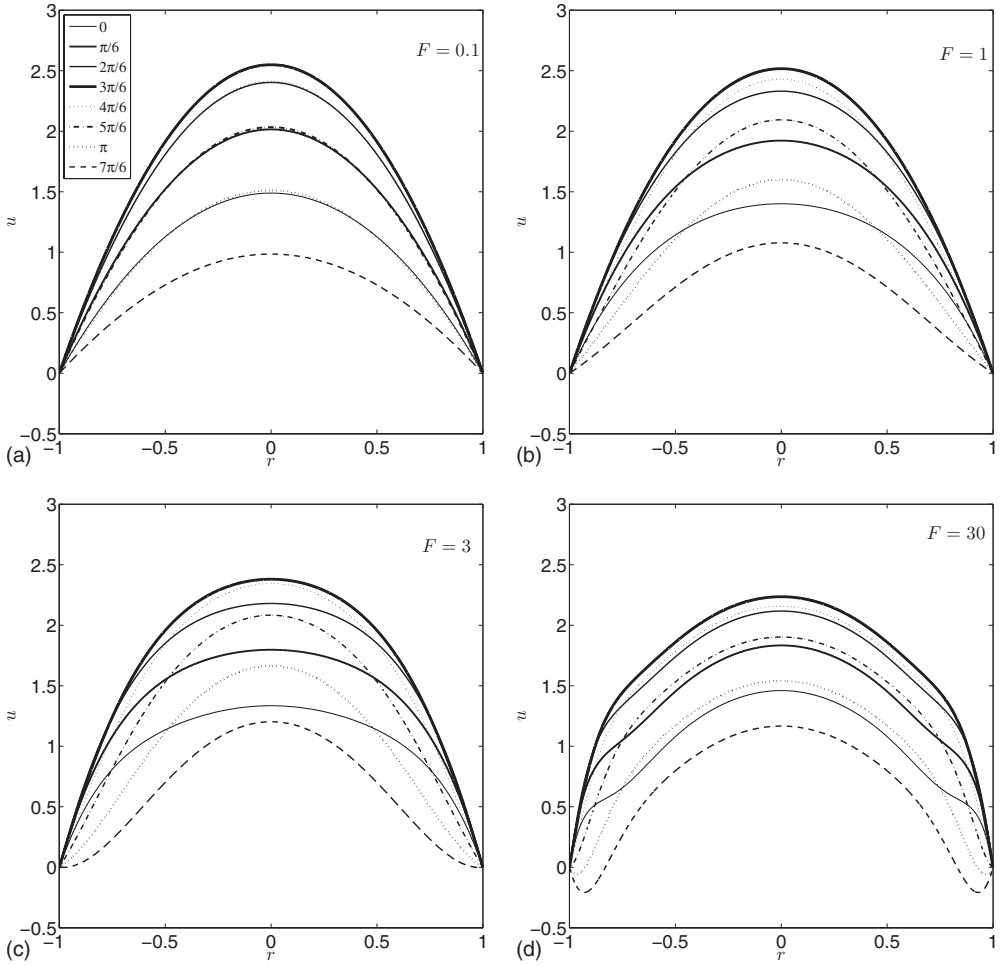

FIG. 3. Velocity profiles at different phase angles for $\dot{m}_A=0.7$ and $F=0.1$, 1, 3, 30 for channel flow.

C. Wall shear stress

The variation in amplitude ratio, between the amplitudes of mass-flow rate $\dot{m}_A$ and shear stress $\tau_{w,A}$, $\dot{m}_A/\tau_{w,A}$ and phase difference $\Delta\theta_\tau$ for channel and pipe flow is presented in Fig. 6. As for the pressure field, low, medium, and high frequency regimes can be identified. Considering the intermediate regime, it is clearly seen from Fig. 6 that the amplitude ratio in the case of channel flow is lower than that for pipe flow. Furthermore, the phase shift $\Delta\theta_\tau$ in the same regime is higher for channel flow. For both cases, $\Delta\theta_\tau$ asymptotically tends to $\pi/4$.

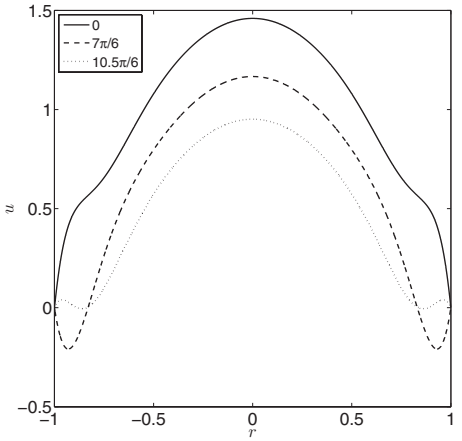

FIG. 4. Velocity profiles indicating no reversal (solid line), near wall reversal (dashed line), reversal away from the wall with two inflection points (dotted line) for $\dot{m}_A=0.7$ and $F=30$ in channel flow.

The maximum and minimum values of the normalized wall shear stress are important parameters especially for the deposition removal in conduits and stent application in blood vessels. Accordingly, as next, the variation in the maximum $\tau_{w,\max}$ and minimum $\tau_{w,\min}$ dimensionless wall shear stress with F was studied for channel and pipe flows. It can be seen in Fig. 7 that $\tau_{w,\max}$ increases with increasing F, while $\tau_{w,\min}$ decreases. The behavior of the investigated quantities can be attributed to the increment of the dimensionless wall shear stress amplitude, τ_A, with F. Furthermore, increasing $\dot{m}_A$ at some pulsation frequency will cause $\tau_{w,\max}$ to increase and $\tau_{w,\min}$ to decrease.

It can be deduced from Fig. 7 that for very low frequencies, $\tau_{w,\max}$ for both cases are equal, while for higher frequencies, the maximum dimensionless wall shear stress for channel flow is larger than that for pipe. Similarly, the values of $\tau_{w,\min}$ are equal at very low frequencies and, at higher frequencies, wall shear stress reaches lower values in the

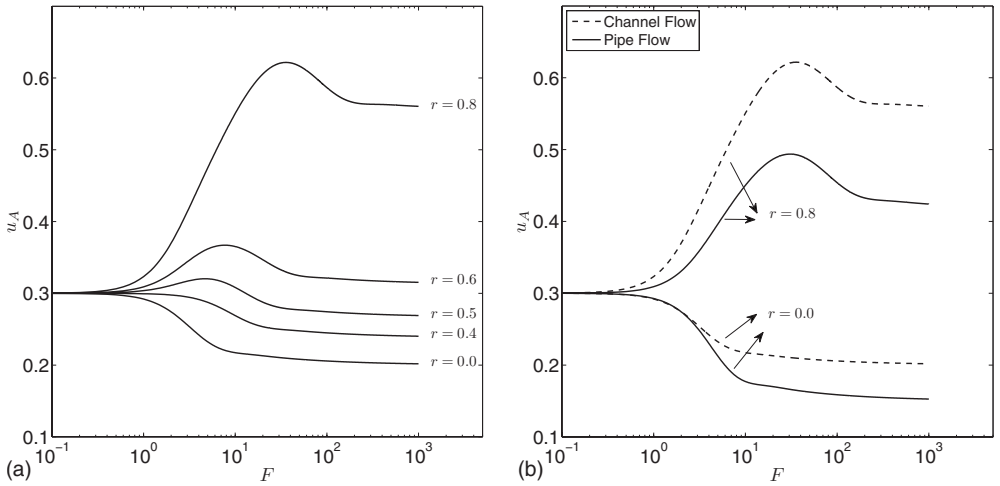

FIG. 5. (a) The variation in the normalized velocity amplitude u_A with the dimensionless frequency F with $\dot{m}_A=0.3$ for $r=0$, 0.4, 0.6, 0.8 in the channel. (b) Comparison of both channel (dashed line) and pipe flows (solid line) for the variation in normalized velocity amplitude u_A with dimensionless frequency F.

channel than those in the pipe. Recently, pulsating flows are used in both removal and prevention of deposits within the piping used in the processing of biomaterial [1]. In such applications, this kind of analysis can be directly utilized to determine the pulsation properties. For example, a threshold wall shear stress for given deposit and thermal state can be quantified beforehand, and utilizing Fig. 7, one can determine the necessary frequency and the pulsation amplitude. Similarly, deposition in blood vessels and relevant issues on the application of the stents in blood vessels can be better understood.

IV. FLOW REVERSAL IN PULSATILE FLOW

Flow reversal is a relevant phenomenon for flow rate metering, entrainment, mixing and separation of species problems. Measurement of the reversal flow is also monumental in the medical application, for example, cerebrospinal fluid motion in the brain [18] and uterine artery blood flow during uterine contractions [19]. In this present section, we are interested in studying quantitatively the eventuate of reversal flow with various flow parameter effects.

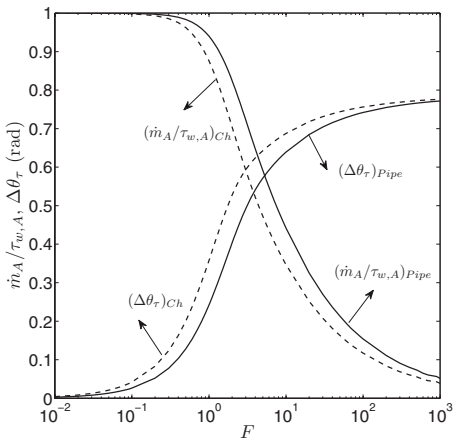

FIG. 6. Comparison between the variation in amplitude ratio, $\dot{m}_A/\tau_{w,A}$, and phase shift $\Delta\theta_\tau$ with F for both channel (dashed line) and pipe flows (solid line).

A. Flow reversal location

In Sec. III B, it has been shown that for some frequency and amplitude of mass-flow rate or of pressure gradient pulsation, flow reversal can occur in two forms in a pulsating flow: wall-attached-reversal [Fig. 4(b) at $7\pi/6$] and off-wall-reversal [Fig. 4(b) at $10\pi/6$]. To the authors' knowledge, the off-wall-reversal has not been reported before. So, finding the locations of the reversal flow is indeed necessary and this may depend on frequency, amplitude of mass-flow rate, as well as the phase angle.

The reversal locations are obtained by finding the roots of the pulsating velocity given in Table I. As the velocity is a transcendental function, so finding the roots in an interval (in the present case, [0,1]) is only possible through numerical methods. For this purpose, we have employed the numerical algorithm given by Boyd [33] using MATLAB. This algorithm is based on the expansion of Chebyschev polynomial series on the canonical interval $[-1,1]$. As this new algorithm gives all the roots within the given domain, so we are able to solve the problems of finding the real roots for this transcendental velocity profile. Due to the no-slip condition, $r=1$ is one of the roots. Therefore, the reversal location r_{rev} are considered to be the root(s) other than the wall. The variation in reversal location r_{rev} at different phases $(2\pi F\tau)$ in one pulsation period are plotted in Figs. 8(a) and 8(b) for channel and pipe, respectively, for different frequencies F at a given mass-flow amplitude $\dot{m}_A=0.7$. Analysis of Fig. 8 shows that with increasing phase angle, the reversal location moves toward the center and then back in the direction of the wall. The appearance of off-wall-reversal reveals itself with a second r_{rev}. The second r_{rev} is indicated by the dashed lines in Figs. 8(a) and 8(b). Moreover, it indicates that for the same flow parameters $\dot{m}_A$ off-wall-reversal begin to appear for $F=5$ in the channel

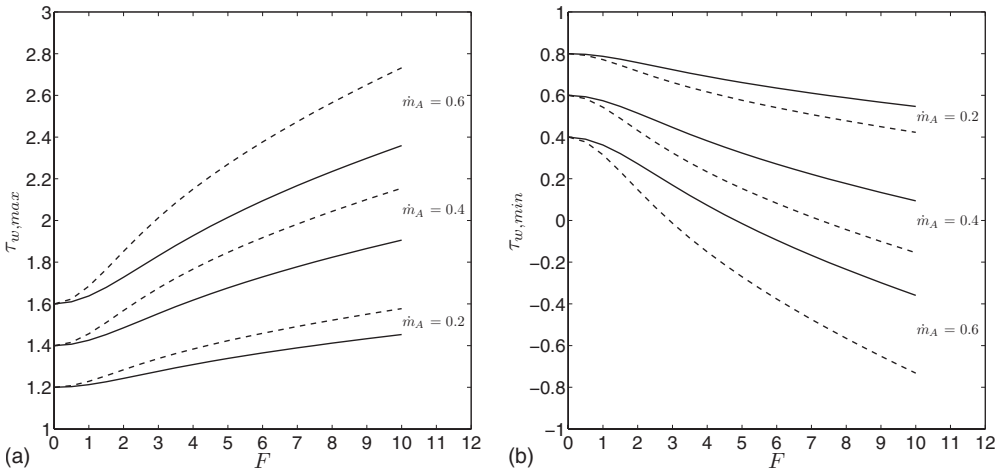

FIG. 7. The variation in the maximum and minimum dimensionless wall shear stress with F at $\dot{m}_A=0.2,\ 0.4,\ 0.6$. Dashed and solid lines represent channel and pipe flow respectively.

flow, whereas only the wall-attached-reversal observed in the case of pipe flow.

It can be deduced from Fig. 8 that for every dimensionless frequency, there is a minimum radial location ($r_{\mathrm{rev,min}}$) at which reversal happens during some phases of the whole cycle. This location is a measure of the penetration of flow reversal in the central region of the conduit. The dependency of $r_{\mathrm{rev,min}}$ on the pulsation parameters is plotted in Fig. 9. It is readily seen in this figure that for both channel and pipe flows, as F increases, the minimum reversal location become closer to the center until some value of F, and then it begins to move away from it. Figure 9 also shows that for the same applied mass-flow rate and pulsation frequency, flow reversal penetrates more to the central region in the channel flow as compared to the pipe flow.

B. Critical conditions for flow reversal and reversal map

The occurrence of flow reversal depends mainly on the pulsation frequency, F and on the dimensionless amplitude of the applied mass-flow rate, $\dot{m}_A$, or, equally, on the amplitude of the pressure gradient pulsation. Since the shear stress vanishes along the change in the flow direction, so the flow reversal occurs when $\partial u/\partial r \leq 0$. Since it is observed that the flow reversal commences at the wall [see Figs. 3(c) and 3(d)], in order to obtain an analytical limiting condition for flow reversal the shear stress (velocity gradient $\partial u/\partial r$) at the wall $r=1$ can be set to zero. For the prescribed sinusoidal mass-flow rate pulsating flows, following from Table I, we get

$$1 + \tau_{w,A} \sin(2\pi F\tau + \Delta\theta_\tau) = 0. \tag{21}$$

with $\tau_{w,A}=\dot{m}_A\frac{|\psi_s|}{|\psi_m|}$, where ψ_s and ψ_m are only functions of the pulsation frequency F. From Eq. (21), one may obtain critical mass-flow rate $\dot{m}_{A,\mathrm{crit}}$ considering that velocity gradient may remain negative for some phase interval, as

$$\dot{m}_{A,\mathrm{crit}} = \frac{|\psi_m|}{|\psi_s|}.$$

In other words, the flow reversal occurs for $\dot{m}_A > \dot{m}_{A,\mathrm{crit}}$ for some period of time of the pulsating wave.

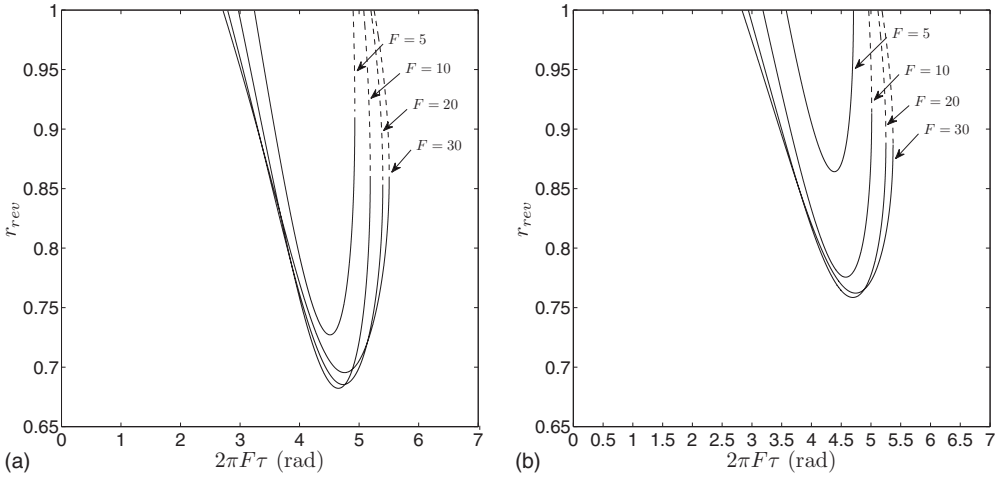

FIG. 8. The variation in the reversal location r_{rev}, with the flow phase (a) for channel flow, (b) for pipe flow at $\dot{m}_A=0.7$. Solid lines and dashed lines are corresponding to the existence of first and second inflection points in the velocity profiles respectively.

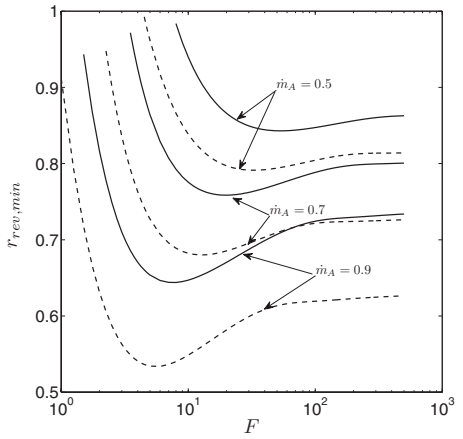

FIG. 9. Comparison between the variation in the dimensionless minimum reversal location with F for both channel and pipe flows. Dashed and solid lines are corresponding to channel and pipe flow respectively.

Figure 10 shows the critical conditions for flow reversal for both channel and pipe flows. Two regions are defined, flow reversal region and no flow reversal region. It is clear from the map that for high $\dot{m}_A$ values, the reversal occurs at low F, while in order to have reversal at low $\dot{m}_A$, extremely high F is needed. The map shows also that for the same $\dot{m}_A$, the applied pulsation frequency for the pipe must be higher than that for the channel flow. This result can also be deduced from Fig. 7, taking into consideration that reversal happens when $\tau_{w,\min}$ attains a zero value. Moreover, for the off-wall-reversal, shown by dashed lines in Fig. 10, one needs higher F at a given $\dot{m}_A$. This off-wall-reversal map has been obtained, using the numerical algorithm explained above [33], by examining the onset of frequency at which the existence of off-wall-reversal locations obtained in any phase of the pulsating period for each prescribed $\dot{m}_A$.

C. Flow reversal amplitude and its duration

In order to get a deeper understanding of flow reversal, further investigations are performed to study the variation in the dimensionless reversal amplitude $u_{A,\mathrm{rev}}$ with r and the effect of F on the dimensionless reversal duration τ_{rev}. At a radial location, $u_{A,\mathrm{rev}}$ is defined as the maximum reversed velocity, and τ_{rev} is described as the period over which the flow is reversed during the whole pulsating cycle. They are computed from the dimensionless pulsating velocity (u) given in Eq. (16). The dependency of $u_{A,\mathrm{rev}}$ on the axial dimensionless location is presented in Fig. 11. As r increases, the dimensionless reversal amplitude increases up to a radial location and then begins to decrease gradually. This behavior is the same for all values of F and $\dot{m}_A$. The location for which $u_{A,\mathrm{rev}}$ reaches its maximum value approaches the wall slightly as F increases for both channel and pipe flows [see Figs. 11(a) and 11(b)]. Unlike the effect of increasing F, Figs. 11(c) and 11(d) clearly depict that increasing $\dot{m}_A$ causes the location for maximum $u_{A,\mathrm{rev}}$ to move away from the wall. It is also observed from Figs. 11(c) and 11(d) that at any reversal radial location, $u_{A,\mathrm{rev}}$ increases with increasing $\dot{m}_A$. However, $u_{A,\mathrm{rev}}$ becomes larger as F increases except at the beginning of the reversal radial locations r [see Figs. 11(a) and 11(b)].

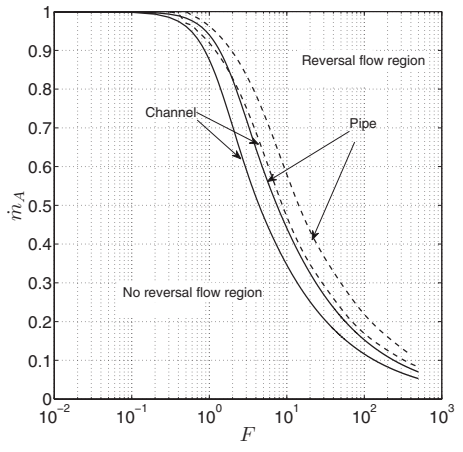

FIG. 10. Regions of flow reversal for both channel and pipe flow as a function of F and $\dot{m}_A$. Solid and dashed lines are corresponding to wall-attached and off-wall reversal.

Figure 12 shows the variation in reversal duration with F for different values of $\dot{m}_A$, and it is observed that the higher the value of F, the longer the reversal duration. This finding is consistent with the results presented in Fig. 8. Comparing the results that were obtained for both channel and pipe flows, it can be concluded that for the same conditions, both $u_{A,\mathrm{rev}}$ and τ_{rev} are higher in the case of channel flow.

D. Reversed mass-flow rate and total reversed mass

During one pulsation cycle and when reversal occurs, the reversal location changes with the phase angle $(\theta = 2\pi F\tau)$ (see Fig. 8). This means that the reversed mass-flow rate $\dot{m}_{\mathrm{rev}}$ is changing with the phase angle. In order to estimate dimensionless $\dot{m}_{\mathrm{rev}}$ (which is normalized with the mean flow rate), the normalized velocity solution (u) is integrated on the cross sectional area as follows:

$$\dot{m}_{\mathrm{rev}} = \begin{cases} \displaystyle\int_{r_1}^{r_2} u\,dr & \text{for channel,} \\ \displaystyle 2\int_{r_1}^{r_2} ru\,dr & \text{for pipe,} \end{cases} \tag{22}$$

where r_1 and r_2 are the reversal locations close to the center and to the wall, respectively. In the case of wall-attached-reversal, r_2 is nothing but the wall itself. The integrations in Eq. (22) are evaluated exactly after finding the reversal locations r_1 and r_2 with the numerical algorithm explained before. The relation between the absolute value of reversed mass-flow rate $|\dot{m}_{\mathrm{rev}}|$ and the phase is plotted in Fig. 13. It can be seen that $|\dot{m}_{\mathrm{rev}}|$ increases with phase angle until it attains a maximum value then it decreases. This can be attributed to the fact that as the phase angle increases, the reversal location moves toward the center and then it travels back to the wall. For both channel and pipe flows, the maximum reversed mass-flow rate attains at the same phase angle where the minimum reversal location occurs (see Fig. 8). For small frequencies F, $|\dot{m}_{\mathrm{rev}}|$ is always higher in channel flow

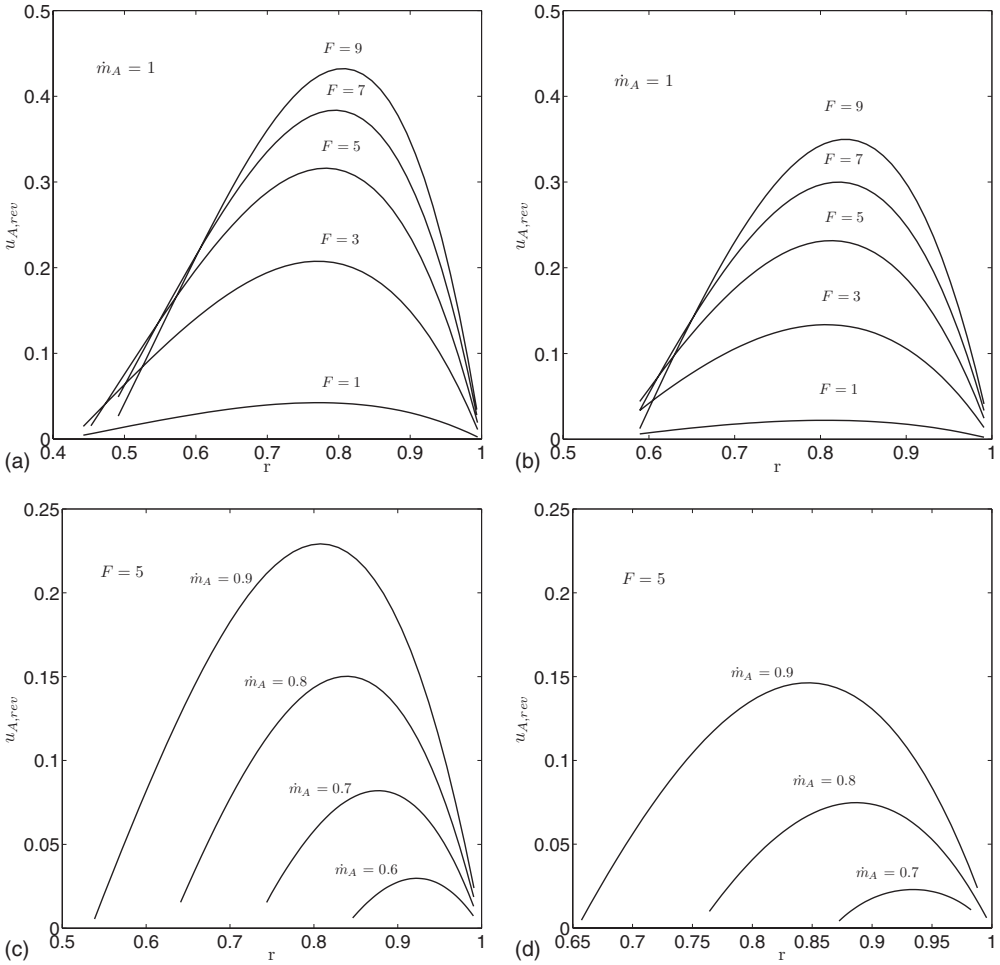

FIG. 11. (a) and (b), the variation in the dimensionless amplitude of reversal with r at $F=1,\ 3,\ 5,\ 7,\ 9$ with a fixed $\dot{m}_A=1$ for channel and pipe flow respectively. (c) and (d), the variation in the dimensionless amplitude of reversal with r at $\dot{m}_A=0.6,\ 0.7,\ 0.8,\ 0.9$ with a fixed $F=5$ for channel and pipe flow respectively.

than that in the pipe flow, but for higher F, e.g., $F=20,30$, $|\dot{m}_{\text{rev}}|$ is lower for channel than pipe flow in some phase angle interval.

The flow reversal would enhance transverse momentum transport, therefore, the total reversed mass (m_{rev}) can be very relevant when two or more species are mixed by pul-

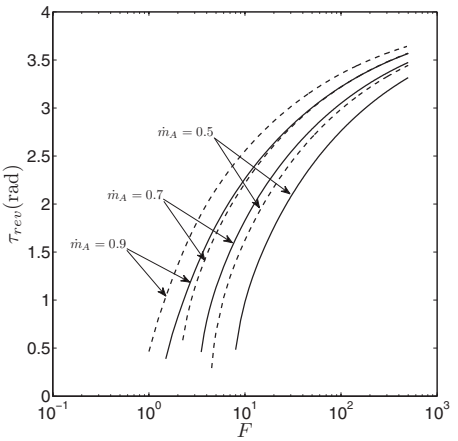

FIG. 12. Comparison between the variation in the reversal duration in phase angle with F for both channel and pipe flows. Dashed and solid lines are corresponding to channel and pipe flow respectively.

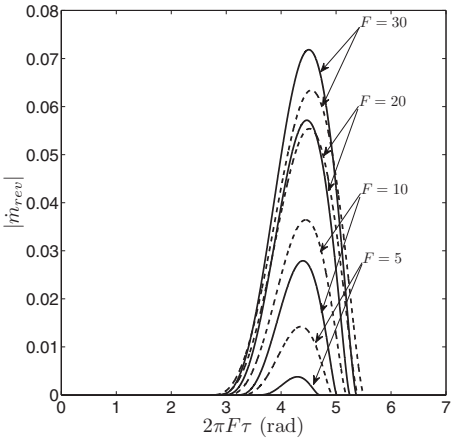

FIG. 13. Comparison between the variation in the absolute value of reversed mass-flow rate with phase angle for both channel and pipe flows at $F=5,\ 10,\ 20,\ 30$ for $\dot{m}_A=0.7$. Dashed and solid lines are corresponding to channel and pipe flow respectively.

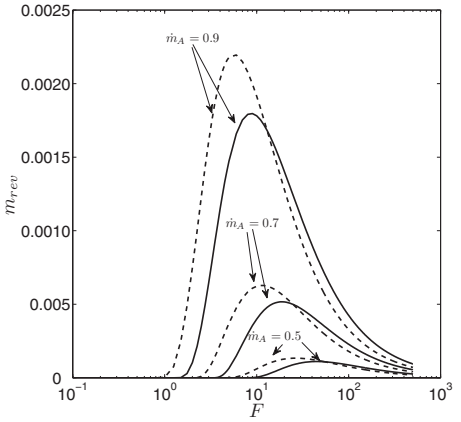

FIG. 14. Comparison between the variation in m_{rev} with F for both channel and pipe flows. Dashed and solid lines are corresponding to channel and pipe flow respectively.

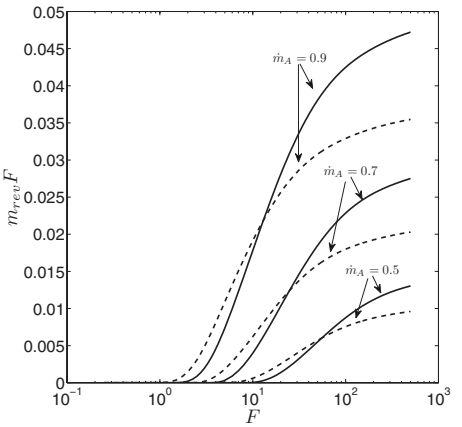

FIG. 15. Comparison between the variation in the percentage of reversed mass to the total mass during the whole cycle with F for both channel and pipe flows. Dashed and solid lines are corresponding to channel and pipe flow, respectively.

sating flow. The total reversed mass m_{rev} is obtained by integrating $|\dot{m}_{\text{rev}}|$ in one pulsating cycle,

$$m_{\text{rev}} = \int_0^{1/F} |\dot{m}_{\text{rev}}| d\tau = \frac{1}{2\pi F} \int_0^{2\pi} |\dot{m}_{\text{rev}}| d\theta. \tag{23}$$

Figure 14 shows m_{rev} as a function of F for different amplitudes of mass-flow rate pulsations. An interesting observation is that m_{rev} has a maximum value for a given mass-flow rate amplitude. With increasing $\dot{m}_A$, the maximum of m_{rev} gets higher and occurs at lower F. Moreover, it can be seen that m_{rev} of the channel flow is only higher than that of the pipe flow at low F. This change in the behavior between pipe and channel flows can readily be observed in Fig. 13: for $\dot{m}_A = 0.7$, the area under the curve for $F=5$ and 10 is more in the case of channel flow than that of the pipe flow, while for $F=20$ and 30 the areas are less. Hence, using Fig. 14, one can choose optimum pulsation parameters which would maximize flow reversal. The dimensional reversed mass can be calculated by multiplying the right hand side of Eq. (23) with the mean mass-flow rate $\dot{m}_M$ and the characteristic time t_c. This dimensional reversed mass can be normalized with the total mass $m_{\text{tot}} = \dot{m}_M / f$ in order to give the percentage of reversed mass to the total mass in one pulsation cycle. After some algebra with the dimensional analysis, $m_{\text{rev}}F$ gives the percentage of reversed mass in one pulsation cycle. As can be seen in Fig. 15, contrary to m_{rev}, the percentage of reversed mass per cycle increases continuously with increasing F.

V. CONCLUSION AND DISCUSSION

Analytical treatments made the interdependency between all flow variables apparent. This clear interdependency in the analytical solution of the pulsating flow problem implies that time series of one of these variables, such as velocity at a known position, wall shear stress, or pressure gradient, would be sufficient to calculate the whole velocity profile and all the other variables. The analytical solution for the sinusoidally pulsating channel flow solution is confirmed experimentally by measuring the time series of the velocity at the center of a channel, in which the mass-flow rate pulsations were well-defined via a mass-flow rate controller [32].

The scaling laws for dimensionless pulsation amplitudes of velocity, mass-flow rate, pressure gradient, and wall shear stress were analyzed for pipe and channel flows as functions of dimensionless frequency of a sinusoidal pulsation. Detailed analysis of flow reversal was conducted. A second type of reversal, which is elevated from the wall, was detected and called as *off-wall-reversal* by the authors. A flow reversal map was provided, showing under which dimensionless frequency and pulsation amplitude wall-attached and off-wall reversal occurs. Further analysis of reversal have shown that for a given mass-flow rate amplitude, there is a certain frequency at which reversed total mass reaches a maximum.

The provided analytical solutions and the results are strictly limited to laminar state of the flow. In steady pipe or channel flows, the minimum Reynolds number at which laminar-to-turbulent occurs is around 2000. Nevertheless, depending on the quality of the flow and the wall of the conduit, this Reynolds number can be as much as 10^5 [34]. Transitions studies in pulsating pipe flows [35–39] shows that flow can experience laminar-to-turbulent and turbulent-to-laminar transition during acceleration and deceleration phases of the pulsations. The Reynolds number, at which transition occurs, is a function of the amplitude and the frequency of the pulsation, i.e., velocity gradient in time. In general, one observes higher transitional Reynolds number in the acceleration phase than that of the steady pipe flow. Nevertheless, once turbulence is set in the flow, it might continue to exist at Reynolds numbers lower than the natural transitional Reynolds number of steady pipe flow. Similar to the transition in steady flows, the transitional regimes in pulsating flows are also highly dependent on the flow quality in the flow facility. Hence, selecting the pulsation amplitude such that Re_{max} in the conduit does not exceed 2000, would warrant the applicability of these results in real life applications. When the natural transitional Reynolds number of the flow facility is known, this limit can be extended to this Reynolds number.

There are several technical applications of the analysis provided here. The solutions and the scaling laws can be

employed to measure, for example, the mass-flow rate by measuring the time series of the pressure gradient, or the center line velocity or the wall shear stress waveforms. The wall shear stress is the key parameter for the deposit prevention or removal in the pipe systems, in which hygienic conditions are required, or for medical treatment of blood vessels by stents. Thus, knowing the necessary wall shear stress, one can easily calculate the pulsation parameters which can generate such a stress. The findings about the flow reversal can be very interesting when mixing or separation of species are considered.

ACKNOWLEDGMENTS

The authors greatly appreciate the support received from the Institute of Fluid Mechanics (LSTM), Friedrich-Alexander-University, Erlangen-Nürnberg, K. Haddad is grateful to DAAD for support. Dr. M.Mishra thanks the Alexander von Humboldt Foundation for the financial support. Authors kindly thank Mr. Çagatay Köksoy for his help in programming some numerical parts of the work. Authors thank Dr. Philip Trevelyan for his valuable suggestions in proofreading the manuscript.

[1] W. Augustin and M. Bohnet, Chem.-Ing.-Tech. **73** (9), 1139 (2001).
[2] G. K. Boreskov and Yu. Sh. Matros, Catal. Rev. - Sci. Eng. **25** (4), 551 (1983).
[3] M. R. Khadilkar, M. H. Al-Dahhan, and M. P. Duduković, Chem. Eng. Sci. **54**, 2585 (1999).
[4] J. D. Jackson, O. Büyükalaca, and S. He, Int. J. Heat Fluid Flow **20**, 115 (1999).
[5] H. N. Hemida, M. N. Sabry, A. Abdel-Rahim, and H. Mansour, Int. J. Heat Mass Transfer **45**, 1767 (2002).
[6] E. P. Valueva, High Temp. **43**, 203 (2005).
[7] P. C. Chatwin, J. Fluid Mech. **71**, 513 (1975).
[8] R. Smith, J. Fluid Mech. **114**, 379 (1982).
[9] A. M. Thomas and R. Narayanan, Ann. N. Y. Acad. Sci. **974**, 42 (2002).
[10] S. Große and W. Schröder, M. Klaas, A. Klöckner, J. Roggenkamp, Experiments in Fluids **42**, 955 (2007).
[11] J. B. Grotberg, Annu. Rev. Biomed. Eng. **3**, 421 (2001).
[12] G. Wolff, L. Eberhard, J. Guttmann, W. Bertschmann, J. Zeravik, and M. Adolph, in *New Aspects on Respiratory Failure*, edited by E. Rögheimer (Springer-Verlag, Berlin, 1992), pp. 235–252.
[13] K. G. Hickling, Am. J. Respir. Crit. Care Med. **158**, 194 (1998).
[14] L. W. J. Bogert and J. J. Van Lieshout, Exp. Physiol. **90**, 437 (2005).
[15] G. F. Mitchell and M. A. Pfeffer, Curr. Opin. Cardiol. **14**, 361 (1999).
[16] K. N. Beronov and F. Durst, Z. Med. Phys. **15**, 257 (2005).
[17] A. Ündar, Med. Sci. Monit. **8**(, ED21 (2002).
[18] A. A. Linninger, C. Tsakiris, D. C. Zhu, M. Xenos, P. Roycewicz, Z. Danziger, and R. Penn, IEEE Trans. Biomed. Eng. **52**, 557 (2005).
[19] H. Li, S. Gudmundsson, and P. Olofsson, Ultrasound Obstet. Gynecol. **22**, 578 (2003).
[20] M. Y. Gündogdu and M. Ö. Çarpınlıoglu, JSME Int. J. **42** (3), 384 (1999).
[21] B. Ünsal, S. Ray, F. Durst, and Ö. Ertunç, Fluid Dyn. Res. **37**, 317 (2005).
[22] D. Das and J. H. Arakeri, J. Appl. Mech. **67** (2), 274 (2000).
[23] G. J. Brereton and Y. Jiang, Phys. Fluids **18**, 103602 (2006).
[24] G. J. Brereton, Phys. Fluids **12**, 518 (2000).
[25] J. Majdalani and H. A. Chibli, Third AIAA Theoretical Fluid Mechanics Meeting, 2002 (unpublished), p. 2981.
[26] D. E. Muntges and J. Majdalani, Third AIAA Theoretical Fluid Mechanics Meeting, 2002 (unpublished), p. 2856.
[27] S. Ray, B. Ünsal, F. Durst, Ö. Ertunç, and O. A. Bayoumi, ASME J. Fluids Eng. **127**, 405 (2005).
[28] S. Uchida, Z. Angew. Math. Phys. **7**, 403 (1956).
[29] S. Ray and F. Durst, Phys. Fluids **16**, 4371 (2004).
[30] R. Akhavan, R. D. Kamm, and A. H. Shapiro, J. Fluid Mech. **225**, 395 (1991).
[31] F. Durst, B. Ünsal, S. Ray, and D. Trimis, Meas. Sci. Technol. **18**, 790 (2007).
[32] K. Haddad, Ph.D. thesis, Friedrich-Alexander-Universität Erlangen-Nürnberg, 2009 (unpublished).
[33] J. P. Boyd, Appl. Numer. Math. **56**, 1077 (2006).
[34] W. Pfenninger, in *Boundary Layer and Flow Control*, edited by G. V. Lachman (Pergamon, New York, 1961).
[35] Ö. Ertunç, B. Ünsal, S. Ray, and F. Durst, Proceedings of the Eurotherm 74th Seminar on Heat transfer in Unsteady and Transitional Flows, Eindhoven, The Netherlands, 2003, edited by H. C. Lange and A. A. van Steenhoven (unpublished), p. 165.
[36] F. Durst, U. Heim, B. Ünsal, and G. Kullik, Meas. Sci. Technol. **14**, 893 (2003).
[37] F. Durst, S. Ray, B. Ünsal, and O. A. Bayoumi, ASME J. Fluids Eng. **127**, 1154 (2005).
[38] M. Ohmi, M. Iguchi, and I. Uratha, Bull. JSME **25** (200), 182 (1982).
[39] M. Iguchi and M. Ohmi, Bull. JSME **25** (2008), 1529 (1982).